

# FATIGUE ANALYSIS IN SELECTIVE LASER MELTING: REVIEW AND INVESTIGATION OF THIN-WALLED ACTUATOR HOUSINGS

Hanns A. Stoffregen<sup>1,2</sup>, Katja Butterweck<sup>1</sup>, Eberhard Abele<sup>1,2</sup>

<sup>1</sup> Institute of Production Management, Technology, and Machine Tools (PTW), Technische Universität Darmstadt, Darmstadt, Germany

<sup>2</sup> LOEWE Research Center AdRIA, Darmstadt, Germany

REVIEWED

## Abstract

The versatile applicable selective laser melting (SLM) is a promising manufacturing technology that allows 3-dimensional design freedom for complex and challenging load bearing parts. A specific application of SLM is the production of thin-walled housings for piezoceramic actuators which induce cyclic loads. Although there are investigations on the fatigue behavior of SLM-specimens, wide acceptance of SLM is limited by a lack of knowledge concerning the operating behavior of actual parts. This paper presents a review on existing studies about fatigue life analysis in SLM as well as results from uniaxial high cycle fatigue (HCF) tests of 1.4542 stainless steel as-built and machined specimens with a stress ratio of  $R = 0$ . Due to a lower surface roughness machined specimens show significantly higher fatigue strength compared to as-built ones. The obtained fatigue strength at  $10^7$  cycles of as-built specimens is used as input for fatigue tests of thin-walled actuator housings. Numerical simulation is used to determine the stress distribution of thin-walled as-built actuator housings under specific loads. Results indicate that the thin-walled as-built actuator housing withstand higher peak stresses compared to as-built specimens due to a high stress gradient.

## 1. Introduction

Additive manufacturing (AM) is an emerging field in manufacturing technologies that has the common principle of building up solid parts directly from 3D CAD data by adding material layer by layer. Part-specific tools are not required in these technologies. Additive manufacturing technologies allow the generation of parts which fulfil the properties of final products (Gibson *et al.*, 2010; Huang *et al.*, 2013; Zhai *et al.*, 2014). Among AM technologies, selective laser melting (SLM) has become a relevant production method for manufacturing ready-to-use parts made from metals such as stainless steel, nickel, titanium, and aluminum alloys (Gu *et al.*, 2012). As AM technology SLM enables the following key advantages for innovative products: function optimized and application tailored product design, function integration, mass customization, resource efficiency, and shortened time to market (Grzesiak *et al.*, 2011; Petrovic *et al.*, 2011; Campbell *et al.*, 2012).

In SLM process development relevant research has been conducted to increase the parts' density since it positively affects mechanical properties such as strength and hardness. High density SLM process parameters were developed for various materials such as stainless steel (Kruth *et al.*, 2010), aluminium (Buchbinder *et al.*, 2011), titanium (Kong *et al.*, 2011), and nickel based alloys (Mumtaz *et al.*, 2008). Static material properties of SLM generated parts are comparable to those of conventionally manufactured ones (Zhai *et al.*, 2014). However, as a powder bed based layerwise process SLM parts are accompanied by a high surface roughness which is a critical factor under cyclical loading (Huang and Leu, 2014). The surface roughness of SLM parts is caused by three main effects: (1) the process inherent stair case effect, (2) partially melted powder particles sticking to the surface, and (3) instability of the melt pool (Thijs *et al.*, 2010; Pyka *et al.*, 2013). Post processing operations such as milling or (electrochemical) polishing allow a smoothening of the surface roughness. Nevertheless, any additional process step is contrary to the direct manufacturing principle underlying AM. In addition, for complex parts with internal features a post processing may not be applicable in any case. To exploit the SLM technique as single-step and near net shape manufacturing route, a knowledge base about fatigue behavior of SLM generated parts in their as-built condition is required. So far limited studies on fatigue

analysis of as-built specimens or actual parts exist. The lack of knowledge concerning the fatigue behavior of as-built SLM parts under operational loads represents a barrier of entry for industry into SLM technology.

The aim of this study is to increase the knowledge base about fatigue life of SLM generated as-built specimens and actual parts. Experiments using as-built and machined SLM 1.4542 stainless steel specimens are used to determine the Wöhler-curves up to  $10^7$  cycles. The fatigue strength in the high cycle fatigue (HCF) regime between these two conditions is compared. Based on fatigue testing of as-built specimens the fatigue behavior of SLM generated thin-walled actuator housings<sup>1</sup> in their as-built condition will be analyzed. To estimate the stress distribution within the thin-walled SLM housings under defined loads a numerical simulation model will be used. Prior to the experiments a comprehensive overview about fatigue analysis in selective laser melting of metal parts is given.

## 2. Review of fatigue analysis in selective laser melting

Over the last decade studies in the field of selective laser melting were primarily focused on process qualification, development of new materials and applications. Examples are studies which investigate the application of SLM for manufacturing medical implants with tailored properties (e.g. porosity) (Murr *et al.*, 2009; Bartolo *et al.*, 2012). Only in recent years studies on fatigue analysis of SLM manufactured specimens have been published and set up a further research area.

Fig. 1 summarizes the results from fatigue analysis using Wöhler tests which have been conducted by various research groups. Each data point represents the characteristic knee point of the obtained S-N curves towards the long life fatigue regime. The analysis of existing studies (Table 1) allows the following conclusions:

- *The present studies are limited towards the material selection.* Most fatigue analysis is focused on stainless steel followed by studies on the SLM well approved Ti6Al4V alloy. Both for AlSi10Mg and Hastelloy<sup>®</sup> X one study is known. Independently conducted studies on machined 1.4542 (17-4 PH) stainless steel performed by Sehart and Witt (2010) as well as by Starr *et al.* (2011) show good accordance. Similarly, results of Rafi *et al.* (2013) and Spierings *et al.* (2013) on machined 1.4540

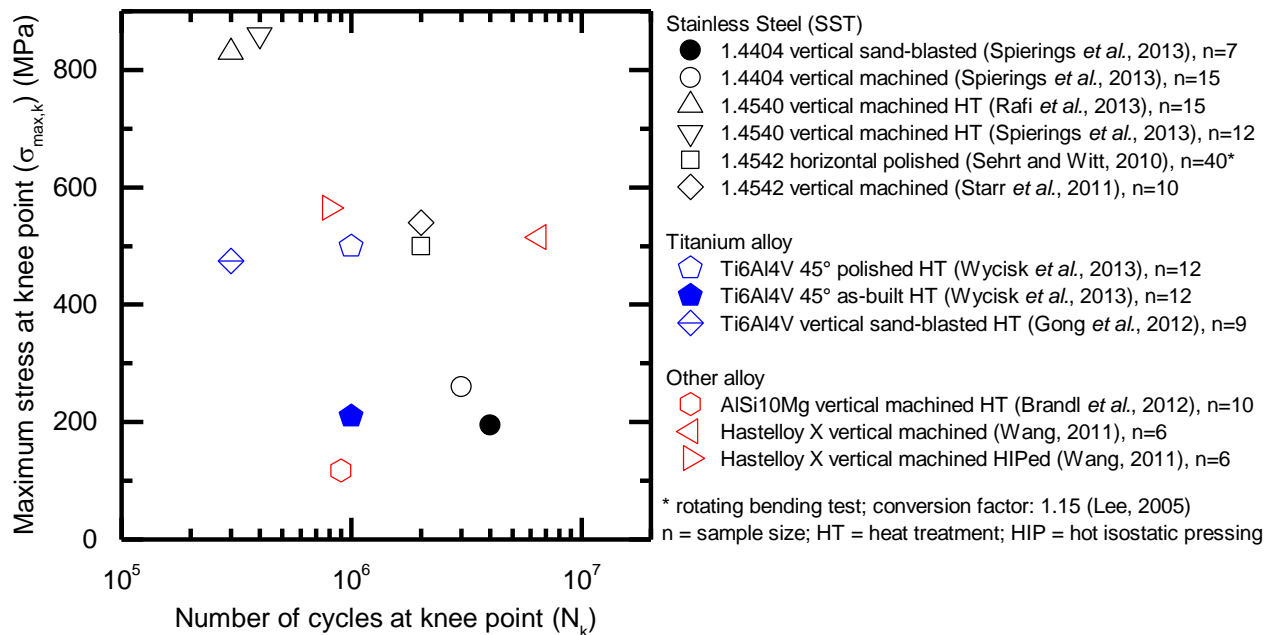


Fig. 1. Summary of knee points (S-N values) from relevant studies on the fatigue life of SLM manufactured specimens.

<sup>1</sup> Function integration is a key advantage of AM technologies. A novel process has been developed to structurally integrate piezoceramic multilayer actuators using the SLM technology (Stoffregen *et al.*, 2013). In this process the actuators are fully integrated into a metallic, monolithic SLM housing. Since the actuator induces cyclic loads knowledge about the fatigue strength of the surrounding housing is required.

(15-5 PH) are comparable towards the fatigue strength at  $10^7$  cycles and the knee point.

- *Studies are primarily focused on the fatigue analysis of post processed SLM specimens.* In most cases for post processing a surface finishing such as turning and polishing was applied. In addition, some studies investigate the influence of subsequent heat treatments. Only three studies on as-built specimens, specifically without surface finishing, could be identified. Spierings *et al.* (2013) investigated different surface treatments on fatigue life of 1.4404 (316L) stainless steel. Between polished and machined specimens no significant difference has been found. In contrast, the as-built specimens showed a lower fatigue strength due to the high surface roughness ( $R_a \approx 10 \mu\text{m}$ ). Results of Wycisk *et al.* (2013) on Ti6Al4V specimens showed a significant difference in fatigue life between as-built and polished specimens as well. The fatigue strength of sand-blasted (Gong *et al.*, 2012) and turned (Rafi *et al.*, 2013) Ti6Al4V specimens show similar values to the results of Wycisk *et al.* (2013) (finished). The number of cycles at the knee points however shows a variance. One reason might be the low sample number of the studies which leads to statistical uncertainty. The research group of Leuders *et al.* (2013) investigated different heat treatments on the fatigue life of Ti6Al4V specimens. A significant positive influence of subsequent heat treatment was observed. In addition, the application of hot isostatic pressing (HIP) could further extend the fatigue life due to reduction of porosity. A similar research design was applied by Riemer *et al.* (2014) on 1.4404 (316L) stainless steel specimens. Besides a heat treatment and a HIP process of machined specimens a set of specimens in their as-built condition was tested. Due to the high surface roughness as-built specimens showed the lowest fatigue strength compared to machined ones. The heat treatment had a positive influence on fatigue life; specimens undergoing a HIP process showed best results. The positive influence of a HIP treatment of SLM generated specimens on fatigue life could be found as well for Hastelloy<sup>®</sup> X by Wang (2012). For AISi10Mg the fatigue strength was determined with and without heat treatment (peak-hardening) on machined specimens (Brandl *et al.*, 2012). A significant positive influence of peak-hardening was observed.
- *The reviewed studies predominantly investigated SLM specimens manufactured vertically under a polar angle of  $0^\circ$ .* Brandl *et al.* (2012) studied three different polar angles ( $0^\circ$ ,  $45^\circ$ ,  $90^\circ$ ) combined with a variation of heat treatment and platform temperature using a DoE approach. The orientation of the specimens had a significant influence on fatigue strength depending on the other two parameters. Above maximum stresses of 600 MPa Hastelloy<sup>®</sup> X specimens showed a higher fatigue resistance when horizontally oriented compared to vertically oriented. Below this stress level the difference was not significant (Wang, 2012). A study on Ti6Al4V specimens manufactured in x, y, and z orientation showed qualitatively better fatigue performance for horizontally than for vertically oriented specimens. However, due to porosity and residual stresses this effect was not quantified (Edwards and Ramulu, 2014).
- *The fatigue life of finished SLM specimens is comparable to conventionally manufactured specimens.* For 1.4404 (316L) little difference in fatigue strength between SLM and conventional specimens was observed (Spierings *et al.*, 2013). A similar conclusion is provided by Sehr and Witt (2010) for 1.4540 (15-5 PH) stainless steel. The study of Rafi *et al.* (2013) on Ti6Al4V showed a higher fatigue strength for SLM specimens compared to cast and annealed specimens due to a fine lamellar microstructure resulting from the SLM process. In general, when comparing fatigue strength of SLM specimens with conventionally manufactured specimens the surface and heat treatment need to be considered (Rafi *et al.*, 2013).
- *Studies on the fatigue behavior of SLM specimens were primarily carried out in the high cycle fatigue regime ( $5 \cdot 10^4 < N \leq 10^7$ ).* Table 1 summarizes the identified studies with corresponding cycle limits and stress ratios. Only the study of Brandl *et al.* (2012) investigated a cycle limit beyond  $10^7$ .
- *The sample size for fatigue tests is between 5 to 15 specimens in one condition.* One exception is the study of Sehr and Witt (2010) which used 40 specimens made from 1.4542 (17-4 PH) stainless steel.

Aside of the tests on fatigue strength, studies on the fatigue crack growth were performed by Riemer *et al.* (2014) on 1.4404 (316L) specimens and the research groups of Leuders *et al.* (2013) and van Hooreweder *et*

al. (2012) on Ti6Al4V specimens. In addition, fatigue analysis on additively manufactured polymers were conducted by van Hooreweder *et al.* (2010), van Hooreweder *et al.* (2013), Blattmeier *et al.* (2012), and Lee and Huang (2013).

A recent study of Lipinski *et al.* (2013) is the only known research work on fatigue analysis of actual parts manufactured using SLM. In their work two different sample sets made from commercially pure grade 2 titanium (CPG2Ti) were tested: 1) thin-walled tube specimens with (w) and without (wo) heat treatment; 2) porous specimens (complex 3D lattice structures with geometrical defined porosity characteristic as bone substitutes (Barbas *et al.*, 2012)). S-N curves for thin-walled tube samples with ( $n = 18$ ) and without ( $n = 40$ ) heat treatment were obtained using a stress ratio of  $R = 0.1$ . The heat treatment showed a negative influence on fatigue limit due to a relaxation of compressive residual stresses. In general, fatigue stress amplitudes between 65.7 MPa (w) and 74.5 MPa (wo) at  $N = 10^7$  found to be relatively low compared to the CPG2Ti bulk material properties. The high surface roughness and SLM specific defects/imperfections were claimed as reasons therefore. For tests on two different porous specimens different cyclic load levels were applied which lead to variations in stress ratio and amplitude. Using this experimental setting a method based on the stress gradient of the structure was developed to define a fatigue criterion for geometrical defined porous structures.

**Table 1.** Overview of studies on fatigue analysis in selective laser melting.

Study	Material	SLM System	Specimens	Research design	Cycle limit / stress ratio
(Sehrt and Witt, 2010)	SST 1.4542 (17-4 PH)	EOS M270	ASTM E466 circular 1	rotating bending test (Wöhler) / polished, horizontally manufactured, without heat treatment / sample size: 40	$N = 10^7$ $R = -1$
(Starr <i>et al.</i> , 2011)	SST 1.4542 (17-4 PH)	EOS M270	ASTM E466 circular 2	tension-tension test (Wöhler) / machined, vertically manufactured, without heat treatment / sample size: 10	$N = 10^7$ $R = 0.1$
(Brandl <i>et al.</i> , 2012)	AlSi10Mg	TrumaForm LF130	ASTM E466 circular 2	tension-tension test (Wöhler) / machined, DoE research design with parameters: (1) building direction ( $0^\circ$ , $45^\circ$ , $90^\circ$ ), (2) platform temperature ( $30^\circ\text{C}$ , $300^\circ\text{C}$ ), (3) heat treatment (no, yes PH T6) / sample size: 9-10 for each condition	$N = 3 \cdot 10^7$ $R = 0.1$
(Gong <i>et al.</i> , 2012)	Ti6Al4V	EOS M270	ASTM E466 circular 2	tension-tension test (Wöhler) / as-built, sand-blasted, with heat treatment / sample size: 9	$N = 10^7$ $R = 0.1$
(Wang, 2012)	Hastelloy® X	EOS M270	ASTM E466 circular / rectangular 1	a) four-point bending test (Wöhler) / machined, vertically and horizontally manufactured, with and without HIP treatment / sample size: 6-9 for each condition b) tension-tension test (Wöhler) / machined, vertically manufactured, with and without HIP treatment / sample size: 6 for each condition	$N = 10^7$ $R = 0.1$ $N = 10^7$ $R = 0.1$
(Chan <i>et al.</i> , 2013)	Ti6Al4V ELI	EOS M270	rectangular	three-point bending test (constant stress amplitude) / two different surface conditions (fully EDM machined/side as-built), horizontally oriented, without heat treatment / sample size: 10 for each condition	$N = \text{n/a}$ $R = 0.1$

Study	Material	SLM System	Specimens	Research design	Cycle limit / stress ratio
(Leuders <i>et al.</i> , 2013)	Ti6Al4V	SLM 250HL	ASTM E466 circular	tension-compression (constant stress amplitude) / machined, vertically manufactured, four different heat treatments / sample size: not specified	$N = 2 \cdot 10^6$ $R = -1$
(Rafi <i>et al.</i> , 2013)	Ti6Al4V	EOS M270	ASTM E466	tension-tension test (Wöhler) / machined, vertically manufactured, with heat treatment / sample size: 9	$N = 10^7$ $R = 0.1$
	SST 1.4540 (15-5 PH)	EOS M270	ASTM E466	tension-tension test (Wöhler) / machined, vertically manufactured, with heat treatment / sample size: 15	$N = 10^7$ $R = 0.1$
(Spierings <i>et al.</i> , 2013)	SST 1.4404 (316L)	Concept Laser MI	ASTM E466 circular 2	tension-tension test (Wöhler) / three different surface conditions (as-built, machined, polished), vertically manufactured, without heat treatment / sample size: 8-15	$N = 10^7$ $R = 0.1$
	SST 1.4540 (15-5 PH)	EOS M270	ASTM E466 circular 2	tension-tension test (Wöhler) / machined, vertically manufactured, with heat treatment / sample size: 12	$N = 10^7$ $R = 0.1$
(Wycisk <i>et al.</i> , 2013)	Ti6Al4V	EOS M270	ASTM E466 circular 2	tension-tension test (Wöhler) / three different surface conditions (as-built, polished, shot-peening), polar angle 45°, with heat treatment / sample size: 12 for each condition	$N = 10^7$ $R = 0.1$
(Edwards and Ramulu, 2014)	Ti6Al4V	MTT 250	rectangular	tension-compression (constant stress amplitude) / as-built and machined surface condition, three different building orientations (x, y, z), without heat treatment / sample size: at least 5 for each condition	$N = 2 \cdot 10^6$ $R = -0.2$
(Riemer <i>et al.</i> , 2014)	SST 1.4404 (316L)	SLM 250HL	ASTM E466 circular	tension-compression (constant stress amplitude) / 1) as-built, 3-4) machined, vertically manufactured, three different heat treatment conditions (without, 650°C, HIPed) / sample size: 5 for each condition	$N = 2 \cdot 10^6$ $R = -1$

The review of studies on fatigue analysis in selective laser melting indicates potential research areas for future work. So far research in the following areas has been of subordinate importance:

- *Investigation of the behavior of SLM parts in the very high cycle fatigue (VHCF) regime:* Load bearing parts in the automotive and aerospace industry are often exposed to cyclic loads beyond  $10^7$  cycles. However, the determination of S-N curves in the HCF regime, which is predominantly existent with respect to SLM, does not necessarily allow an estimation of the very high cycle fatigue behavior since the asymptote must not be horizontally (Bathias, 1999; Marines I. *et al.*, 2003; Sonsino, 2007; Pyttel *et al.*, 2011; Stanzl-Tschegg, 2014). The references indicate that the course of the S-N curves is material dependent. When a so-called “endurance limit” is used for design, the safety against a declining S-N curve in the VHCF regime will decrease (Sonsino, 2007). Based on applications of SLM manufactured parts with loads beyond  $10^7$  cycles relevant studies have to be performed which allow a statistical significant assessment of fatigue strength in this regime.

- *Studies on repeatability of fatigue characteristics:* As shown in Table 1 most Wöhler tests were performed based on 6 to 15 samples which is at the lower end of the recommendation of 12 to 24 samples for design allowable and reliability tests (Lee *et al.*, 2005). With increasing sample size the confidence of the fatigue strength can be increased (Beretta *et al.*, 1995; Martin *et al.*, 2011). In addition, the influence of build direction and position as well as inter and intra batch comparisons have not been studied systematically so far. This might be of further interest, since it is known from other studies that the SLM process is accompanied by anisotropy (Tolosa *et al.*, 2010; Chlebus *et al.*, 2011; Spierings *et al.*, 2013; Thijs *et al.*, 2013) which may also affect the fatigue behavior.
- *Studies on actual parts manufactured by SLM under operational loads:* Present studies follow a standard protocol using uniaxial or bending tests based on specimens. Test series to assess the fatigue behavior of SLM generated parts also under complex (multiaxial, stochastic and/or operational) stress-strain scenarios have not been conducted. In addition, limited knowledge on the fatigue behavior of as-built specimens (e.g. high surface roughness) is present which is of special interest to use SLM as direct single-step manufacturing technology.

### **3. Research methodology**

#### **3.1 System and material**

For the purpose of this study all specimens were manufactured on an EOS M270 SLM system with a 200 W Yb-fibre laser (continuous wave, wave length  $\lambda = 1064$  nm, Gaussian beam profile), using commercially available 1.4542 (17-4 PH) stainless steel powder ( $d_{50} \approx 28$   $\mu\text{m}$ ;  $d_{90} \approx 41$   $\mu\text{m}$ ). The system integrated beam expander was set to a laser spot diameter  $d_s \approx 140$   $\mu\text{m}$ . PRIMES Focus/Beam Monitor is used to verify the laser power output and laser spot diameter. For all specimens, the layer thickness was fixed to 20  $\mu\text{m}$ , representing the default value for the combination of material used and the SLM system. All specimens were manufactured using a meander-shaped stripe exposure which rotates along the z-axis. A qualified exposure parameters which lead to fully dense parts (laser power  $P = 195$  W; scan speed  $v_s = 1000$  mm/s; hatch distance  $h = 0.1$  mm) was applied.

#### **3.2 Uniaxial fatigue test of SLM manufactured specimens**

As test geometry for fatigue analysis common round un-notched specimens ( $K_t = 1.0$ ) according to ASTM E466-07 with tangentially blending fillets between the test section and the ends have been chosen. The nominal diameter was set to 6 mm, the length of the constant test section to 11 mm. All specimens were manufactured vertically oriented. 39 specimens were manufactured in net-shape to be tested as-built, 20 specimens were manufactured with 1 mm allowance and machined afterwards. The as-built specimens were manufactured in two batches. Fatigue tests were performed on an Instron servohydraulic Hydropuls MHF test system at ambient conditions. A uniaxial test setup with a stress-ratio of  $R = 0$  (pulsating tension) and  $N = 10^7$  cycles as the maximum number of cycles was selected. The test frequency was varied between 70 Hz and 140 Hz depending on the applied load. In this regime a significant influence of the test frequency is not expected due to the absence of corrosion induced degradation effects and temperature rise of the specimens (Bargel and Schulze, 2005; Spickenreuther, 2007).

The routine test (Weibull, 1961) in combination with the staircase method (Lin *et al.*, 2001; Morrissey and Nicholas, 2006) was used to determine the S-N curves and the fatigue strength at  $N = 10^7$  cycles. The initial stress of 500 MPa for as-built and 600 MPa for machined specimens has been reduced stepwise until no failure occurred. Afterwards the staircase tests were performed for as-built and machined specimens. Since the as-built specimens were manufactured in two batches the staircase method has been applied for each batch separately. To determine the statistical distribution of the S-N curve each stress horizon has been tested twice for machined and five times for as-built specimens (three from batch one, two from batch two). Analysis of fatigue tests was carried out with a survival probability of 10%, 50%, and 90% using a Gaussian probability grid and the formula of Rossow (1964). The staircase tests were evaluated based on the method proposed by Hück (1983) which takes account of the step interval and the stress horizon of all valid data points. The width of the scatter band has been assumed to be constant after the knee point (Sonsino, 2008).

The roughness of three machined and three as-built specimens has been determined using a contact surface measurement system (Perthometer).

### 3.3 Uniaxial fatigue test of SLM manufactured thin-walled as-built actuator housings

In previous research a process has been developed to fully integrate piezoceramic actuators into a metallic, monolithic housing by means of SLM. The main advantage is an application tailored housing design, particularly the stiffness of the housing (Stoffregen *et al.*, 2013). Therefore, the housing shown Fig. 5a has three design parameters, wall thickness  $t$ , housing radius  $r$ , and angle of bellow  $\alpha$ , which can be adjusted to obtain proper stiffness characteristics. A numerical simulation model has been used to determine the stress distribution within the housings under specific loads. Three different housings have been tested. The selection was based on the fatigue strength obtained from the as-built specimens and the resulting stress distribution under application relevant loads. Application relevant loads were derived from typical blocking forces of integrated actuators (maximum value 1.5 to 2 kN). Fatigue analysis of the thin-walled housings is referred to the peak stress.

The selected housings were tested similarly to the specimens (section 3.2). A uniaxial test setup with a stress-ratio of  $R = 0$  was chosen and corresponds to the load scenario induced by integrated actuators. The maximum number of cycles to be performed was set to  $N = 10^7$  cycles. The test frequency was set to 133 Hz for all thin-walled housings due the low applied forces. For all three housing geometries a routine test method was used. For two housing types 10 samples were tested, for the other one 29 samples. In addition to the routine test the staircase method was used for the latter. Analysis corresponds to the procedure described under section 3.2.

## 4. Results

### 4.1 Fatigue strength of as-built and machined specimens

The arithmetical mean deviation of the roughness profile for as-built specimens is on average  $Ra = 13.7 \mu\text{m}$ , the maximum height of the roughness profile is on average  $Rz = 86.0 \mu\text{m}$ . For machined specimens the roughness parameters are  $Ra = 0.2 \mu\text{m}$  and  $Rz = 1.7 \mu\text{m}$ . Fig. 2 shows the results of the fatigue tests of as-built and machined specimens. Corresponding survival probability levels are included for 10%, 50%, and 90% probability. The calculated fatigue strength at  $10^7$  cycles is  $\sigma_{max} = 219 \text{ MPa}$  for as-built specimens, which corresponds to a stress amplitude of  $\sigma_a = 110 \text{ MPa}$ . For machined specimens the maximum stress at  $10^7$  cycles is  $\sigma_{max} = 492 \text{ MPa}$  ( $\sigma_a = 246 \text{ MPa}$ ). Table 2 summarizes the characteristic parameters of the obtained S-N curves. The slope in the finite life region is significant flatter for machined compared to as-built specimens.

Fig. 3 illustrates the results of the staircase testing method. A fictive test result has been added for as-

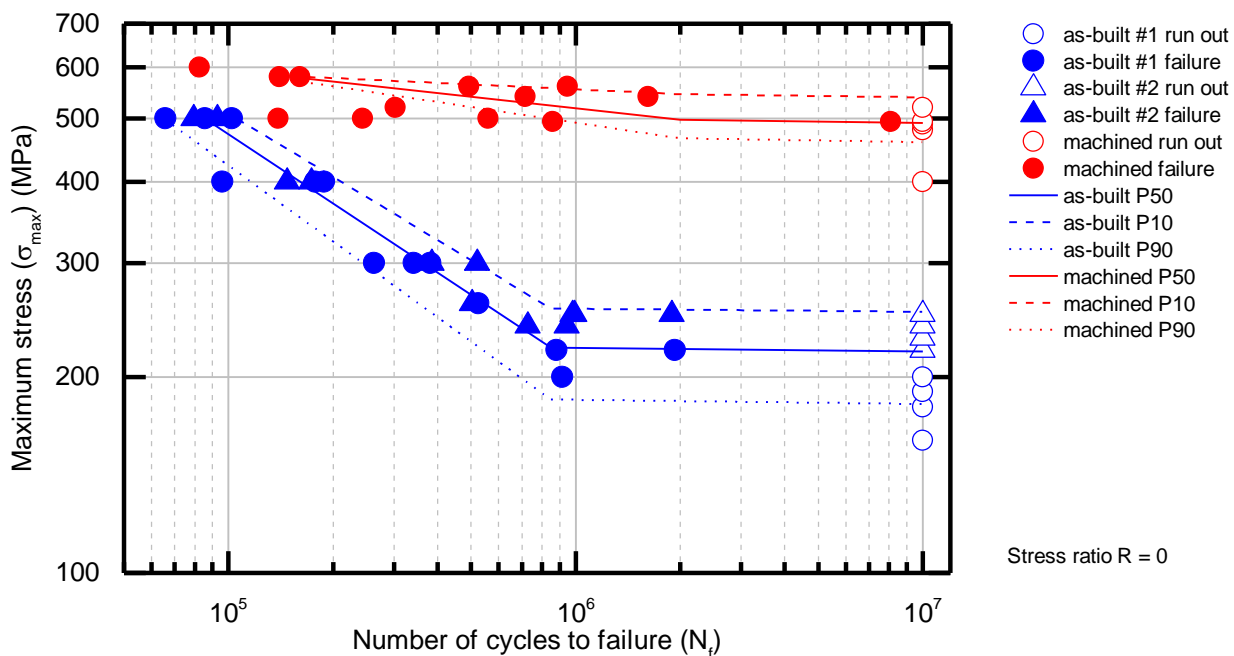


Fig. 2. S-N curves with survival probability for as-built and machined specimens (log-log scale).

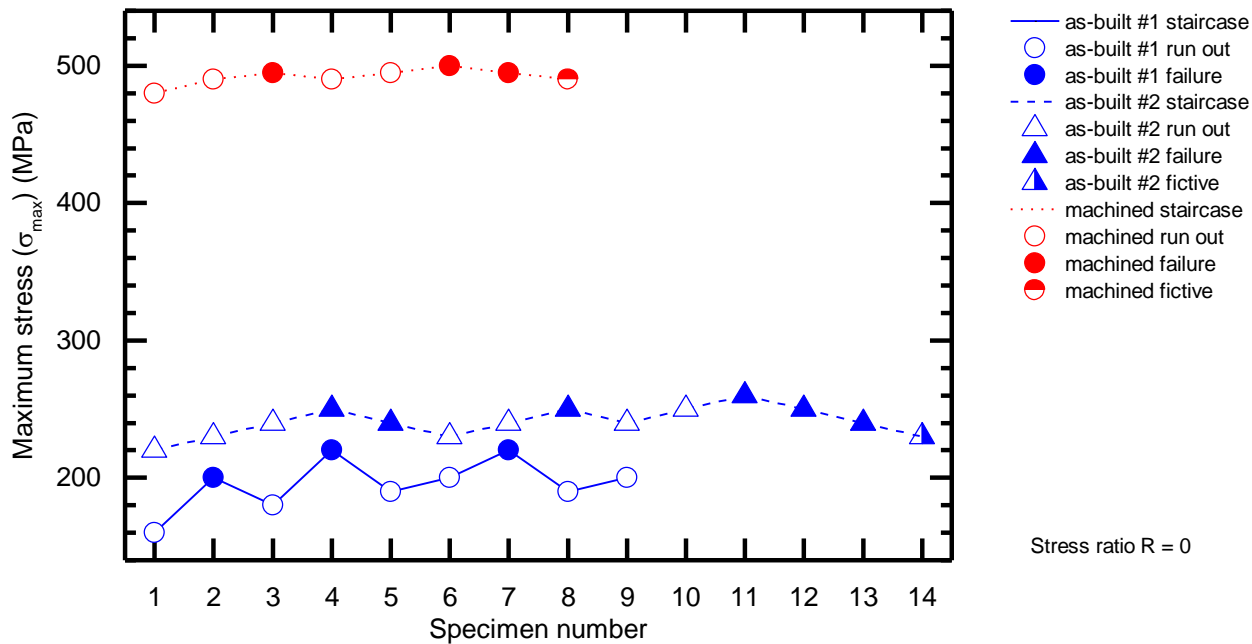


Fig. 3. Staircase testing results for as-built specimens (batch 1 & 2) and machined specimens.

built specimens (batch 2) and machined specimens according to Hück (1983). For as-built specimens the two conducted staircase tests show a divergence of the stress amplitude in the range of 10 MPa. Since manufacturing parameters have not been changed and significant differences in microstructure and hardness among the specimens from batch 1 and 2 have not been observed, both batches are analyzed together. In addition, previous conducted inter and intra batch comparisons on tensile strength of SLM manufactured 1.4542 stainless steel specimens demonstrated reproducibility.

Table 2. Characteristic parameters of the S-N curves for as-built and machined specimens.

Characteristic parameter of S-N curve	As-built (batch 1&2)	Machined
Slope $k$	3	20
$k = \frac{\log(N_k/N_{N10^4})}{\log(\sigma_{N10^4}/\sigma_k)}$		
Knee point		
Number of cycles $N_k$	850,000	2,000,000
Maximum stress $\sigma_{max,k}$	222 MPa	498 MPa
Fatigue strength at $10^7$ cycles (50% probability):		
Maximum stress $\sigma_{max}$ / stress amplitude $\sigma_a$	219 MPa / 110 MPa	492 MPa / 248 MPa
Number of specimens	39	20
Number of run outs	13	6
Horizontal scattering range $T_N$ (arithmetic average)	1.93	2.61
$T_{N,i} = \frac{N_{P90,i}}{N_{P10,i}}$ ; with $i = 1, 2 \dots$		
Vertical scattering range $T_\sigma$ at $N = 10^7$	1.38	1.17
$T_\sigma = \frac{\sigma_{max,P90}}{\sigma_{max,P10}}$		

Optical investigations of all fracture surfaces show that crack initiation starts from the specimens surface (Fig. 4a,c). Only for one machined specimen a crack initiation from a pore/melting defect close to the surface is observed (Fig. 4b). Machined and as-built samples show an obvious elongation in the finite cycle fatigue life

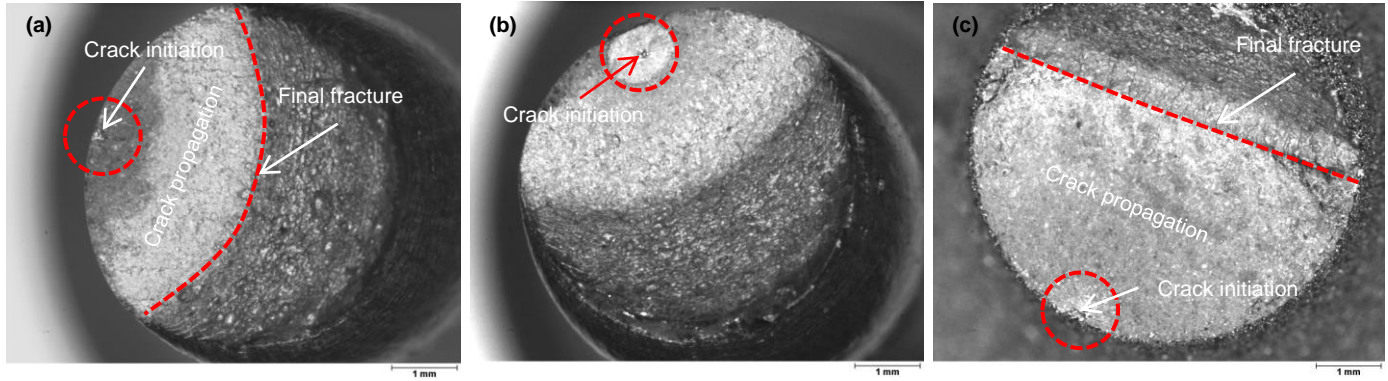


**Fig. 4.** Microscopic images of lower fracture surfaces. a) machined specimen ( $N_f = 860,739$ ;  $\sigma_{max} = 495$  MPa), b) machined specimen ( $N_f = 8,092,655$ ;  $\sigma_{max} = 495$  MPa), c) as-built specimen ( $N_f = 525,654$ ;  $\sigma_{max} = 260$  MPa).

regime. For as-built samples under a load above  $\sigma_{max} = 300$  MPa ( $\sigma_a = 150$  MPa) multiple cracks on the surface can be detected. The final fracture zone for as-built specimens in the HCF range is straight due to a lower stress amplitude and longer crack propagation (Fig. 4c). Contrary, for machined specimens a semi-circular shape is observed (Fig. 4a). Prepared micrographs of machined and as-built specimens showed no significant influence of the post-processing on the microstructure (e.g. surface hardening), which may influence the fatigue strength.

#### 4.2 Fatigue strength of thin-walled as-built actuator housings

The fatigue strength results at  $10^7$  cycles of as-built specimens are used as input for the fatigue analysis of thin-walled as-built actuator housings. An ANSYS mechanical simulation model of the housings is used to determine the geometrical dependent stress distribution under application relevant loads. The design parameters of the housing are wall thickness  $t$ , housing radius  $r$ , and angle of bellow  $\alpha$  (Fig. 5a). Three different housing designs are tested. The selection criterion is based on operational loads which result in a maximum stress (von Mises) close to the fatigue strength at  $N = 10^7$  cycles of as-built samples ( $\sigma_{max} = 219$  MPa). Micrographs of the bellow fold are used to determine the as-produced wall thickness (Fig. 5b). The numerically obtained stress distribution displaying position and value of the maximum stress is shown in Fig. 5c exemplarily for housing 2. Since it is assumed that the housing design results in a notch effect which reduces the fatigue strength one initial housing test is performed with an operational load resulting in a lower maximum stress. Due to a divergence between simulated ( $k_{h,sim}$ ) and experimentally determined ( $k_{h,exp}$ ) housing stiffness a correction of the test load  $F_{test}$  following the equation

$$F_{test} = F_{sim}(\sigma_{max,p}) \cdot \left( \frac{k_{h,exp}}{k_{h,sim}} \right) \quad (1)$$

is conducted. Using this equation a maximum test load can be calculated from an expected maximum peak stress  $\sigma_{max,p}$ . An approximate linear relationship between load and maximum stress is shown during FE analysis. Table 3 summarizes the initial test load for the thin-walled housing as well as relevant design

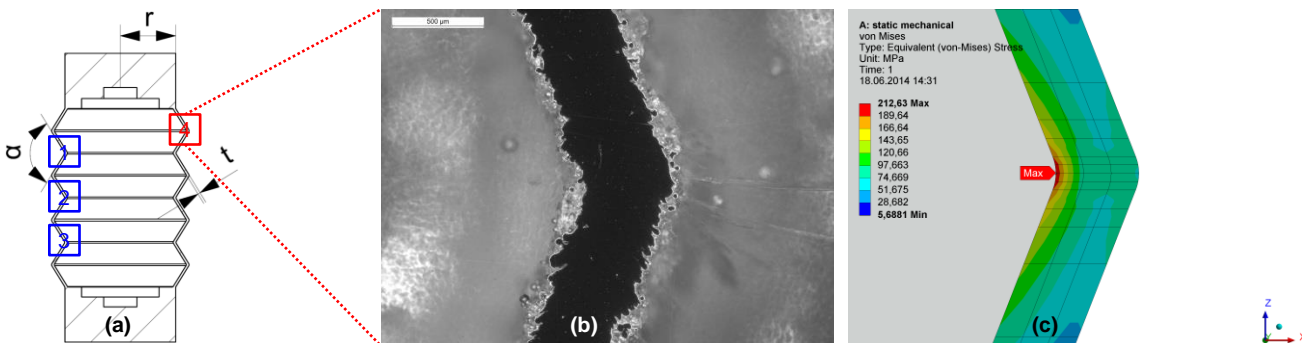


**Fig. 5.** (a) Cross section of the thin-walled actuator housing and design parameters. Numbers indicate position of the bellow. Blue marked are inner folds, red marked is the outer fold at which the numerical simulation shows the highest peak stress. (b) Micrograph of a bellow fold (housing 2); black: cross section of the fold, grey: embedding resin. (c) FEA result of stress distribution in an outer bellow fold for housing 2.

parameters.

**Table 3.** Initial test setup for thin-walled actuator housings and corresponding housing design parameters.

Housing	Test load $F_{test}$	Stress (v. Mises)*	Stiffness $k_{h,sim}$	Stiffness $k_{h,exp}$	Design parameter ( $t, r, \alpha$ )
1	1.85 kN	213 MPa	93 N/ $\mu$ m	84 N/ $\mu$ m	0.6 mm, 8.5 mm, 160°
2	0.76 kN	213 MPa	34 N/ $\mu$ m	25 N/ $\mu$ m	0.5 mm, 10.0 mm, 137.5°
3	0.82 kN	182 MPa	44 N/ $\mu$ m	35 N/ $\mu$ m	0.6 mm, 8.5 mm, 137.5°

\* maximum peak stress ( $\sigma_{max,p}$ ) based on FEA

Fig. 6 shows the results of the fatigue tests of the three different housings designs. The maximum stress (peak stress at notch root) is calculated from the test load using equation (1). The knee point for all tested housings is in the range of  $7.5$  to  $10 \cdot 10^5$  cycles and therewith in a higher cycle regime than the tested as-built specimens. In contrast, the scattering range is below the tested as-built specimens, both horizontally ( $T_N$ ) and vertically ( $T_\sigma$ ). The slopes in the finite life region show little variance among the three housings. Compared to the fatigue strength at  $N = 10^7$  cycles of the as-built specimens the housings withstand a higher maximum stress. When exhibiting failure the cracks occur at one of the three inner folds (Fig. 5a). A predominantly position of the crack among the three inner folds is not observed. Table 4 summarizes the parameters of the S-N curves for the thin-walled housings.

## 5. Discussion

A strong divergence between the fatigue behavior of as-built and machined SLM 1.4542 stainless steel specimens in the HCF regime is observed. For the machined specimens the fatigue strength at  $N = 10^7$  cycles is 492 MPa and accounts 51% of the measured ultimate tensile strength ( $R_m = 961$  MPa). This finding is in accordance to the studies of Sehrt and Witt (2010) and Starr *et al.* (2011) which obtain values of 52% respectively 56%. It is also to notice that the S-N curves in this two studies show comparable parameters (slope, knee point) to the one in this research work. Therefore, reproducibility of fatigue properties of SLM generated specimens can be assumed. The results of Wu and Lin (2002) on conventionally manufactured 1.4542 stainless steel show fatigue strength values in the same magnitude. This finding supports comparability of fatigue

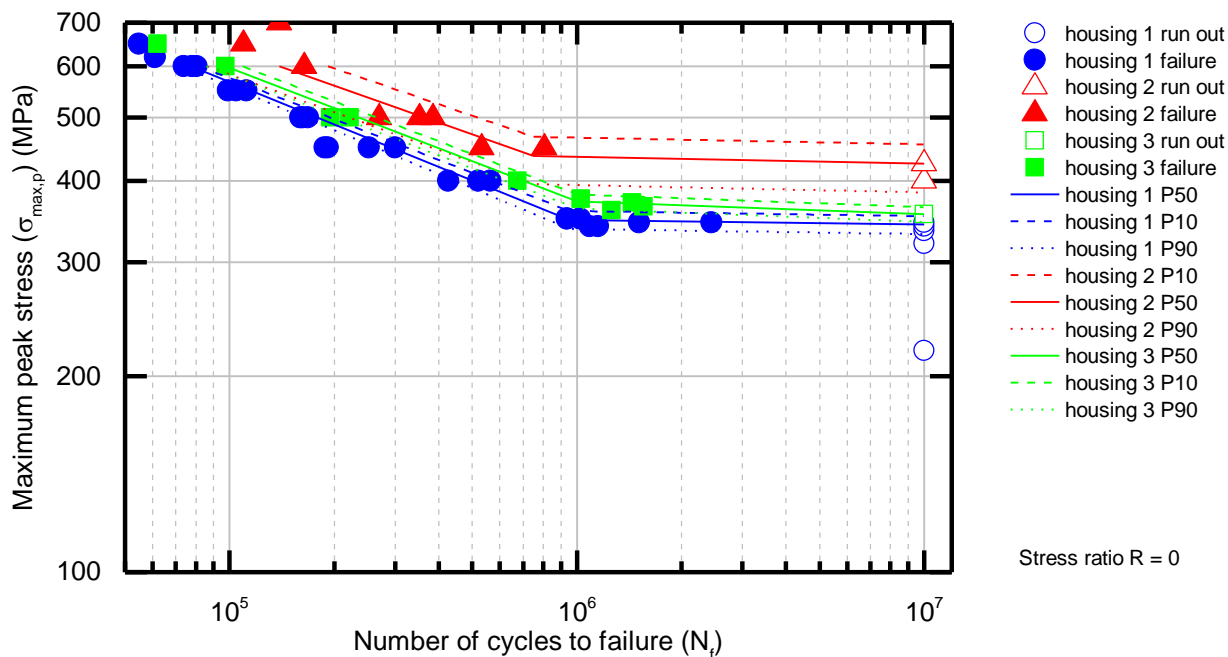


**Fig. 6.** S-N curves with survival probability for thin-walled actuator housings 1-3 (log-log scale). Maximum peak stress is based on v. Mises stress at the notch root.

**Table 4.** Characteristic parameters of the S-N curves for thin-walled actuator housings.

Characteristic parameter of S-N curve	Housing 1	Housing 2	Housing 3
Slope $k$ $k = \frac{\log(N_k/N_{N10^4})}{\log(\sigma_{N10^4}/\sigma_k)}$	4.8	4.8	5.0
Knee point			
Number of cycles $N_k$	950,000	750,000	1,000,000
Maximum stress $\sigma_{max,k}$	348 MPa	437 MPa	372 MPa
Fatigue strength at $10^7$ cycles (50% probability):	343 MPa /	425 MPa /	355 MPa /
Maximum peak stress (v. Mises) $\sigma_{max,p}$ /	172 MPa	213 MPa	178 MPa
Peak stress amplitude (v. Mises) $\sigma_{a,p}$			
Number of specimens	29	10	10
Number of run outs	5	2	1
Horizontal scattering range $T_N$ (arithmetic average)	1.31	1.63	1.28
$T_{N,i} = N_{P90,i} / N_{P10,i}$ ; with $i = 1, 2 \dots$			
Vertical scattering range $T_\sigma$ at $N = 10^7$	1.07	1.19	1.05
$T_\sigma = \sigma_{max,P90} / \sigma_{max,P10}$			

behavior between machined SLM generated specimens and conventional manufactured ones.

For as-built specimens the fatigue strength at  $N = 10^7$  cycles is with 219 MPa significantly below the value of machined specimens. The fatigue strength accounts only 23% of the ultimate tensile strength. The reason can be found in the high surface roughness of as-built specimens and the therewith associated notch effect (Arola and Williams, 2002; Radaj and Vormwald, 2007; Chan *et al.*, 2013). The surface roughness due to partially melted powder particles and the inconsistency of the melt pool causes micro notches at the specimen's surface which lead to a stress intensity during cyclical loadings. The analysis of the fracture surface shows that crack initiation occurs at defects on the specimen's surface and supports this assumption. Based on the fatigue results an experimentally determined surface roughness reduction factor  $\gamma$  in the HCF regime can be calculated:

$$\gamma = \frac{\sigma_{max,N=10^7,as-built}}{\sigma_{max,N=10^7,machined}} = 0.44 \quad (2)$$

For as-built specimens a significant divergence between the two batches is not assumed. The following reasoning underlies this procedure: (1) Divergence between the two batches is only present above  $9 \cdot 10^5$  cycles. In the finite life region the results indicate random scattering. (2) Manufacturing parameters have not been changed and significant differences in microstructure and hardness among the specimens from batch 1 and 2 have not been observed. (3) The vertical scattering  $T_\sigma = 1.38$  in the HCF regime of the combined analysis of batch 1 & 2 is in the range of cast and sintered steel (Sonsino, 2007).

The slope in the finite life region  $k$  as well as the cycle number at the knee point  $N_k$  of machined specimens is typical for un-notched cast and sintered steel with medium strength (Sonsino, 2007). Machined specimens (slope  $k = 20$ ) show a higher sensitivity towards stresses in the finite life region compared to as-built specimens (slope  $k = 3$ ). With increasing notch effect (e.g. surface roughness) the slope becomes steeper and the sensitivity towards stress variations decreases (Lee *et al.*, 2005; Radaj and Vormwald, 2007). This finding is true for the as-built specimens which show a significant steeper slope compared to machined ones; in case of as-built specimens crack propagation mechanisms are dominant.

The fatigue analysis of the thin-walled housings shows that the maximum stress at the notch root is significantly above the value of as-built specimens ( $\sigma_{max} = 219$  MPa). The fatigue strength of the housings at  $N = 10^7$  cycles is between 343 MPa for housing 1 and 425 MPa for housing 2. A potential explanation can be found in the stress gradient. For the parameters shown in Table 3 an FEA is applied to determine the stress

distribution at the folds. The stress gradient at the notch root is calculated according to (Siebel and Stieler, 1955; Filippini, 2000):

$$\chi = \frac{1}{\sigma_{max,p}} \left. \frac{\partial \sigma}{\partial x} \right|_{x=0} \quad (3)$$

The stress gradient and distribution for the three housings are shown in Fig. 7. The stress gradient determines how steep the stress decreases with distance from the notch's root. A low stress gradient results in a higher average stress in the local damage zone. Based on the stress gradient concept higher stress gradients increase fatigue strength since it decreases the volume fraction of highly stressed material (Siebel and Stieler, 1955; Kuguel, 1961; Lee *et al.*, 2005; Adib-Ramezani and Jeong, 2007; Schijve, 2009). For the tested housing the order of the stress gradients is  $\chi_1 < \chi_3 < \chi_2$ . This result implies that housing 1 should have the lowest fatigue strength and housing 2 respectively the highest fatigue strength which is in accordance to the obtained S-N curves in Fig. 6. Therefore, besides peak stresses the stress gradient needs to be considered for fatigue analysis of the thin-walled as-built actuator housings.

Of practical relevance is the little scattering of the test results for the thin-walled actuator housings. Both, horizontal and vertical scattering, are significantly below the ranges of the as-built and machined specimens. This allows a fatigue life approach with a low safety factor.

Based on the FEA results indicating a maximum peak stress at the top outer fold (Fig. 5a, position 4) a failure is assumed to occur at the same position. Contrary when exhibiting failure it occurred at one of the three inner folds (Fig. 5a, positions 1-3). Crack initiation starts from the outer side from one of the three inner folds. A potential explanation is the geometry of the thin-walled housing. Outer folds are characterized by a larger diameter compared to inner folds while having the same wall thickness. Consequently, outer folds have a larger cross section compared to inner folds which results in a lower average stress. The latter might be the reason why the thin-walled housings exhibit failure at the inner folds.

The thin-walled housings demonstrate fatigue strength at  $N = 10^7$  cycles for loads up to 1.5 kN which fulfils the requirements of the proposed application (integration of piezoceramic actuators). For housing 1 fatigue strength at  $10^7$  cycles exists even for loads up to 2.5 kN.

## 6. Summary and outlook

The present work shows a review of fatigue analysis in selective laser melting. Within this comparably new research field studies are conducted almost exclusively on the basis of specimens. The studies focus on SLM approved stainless steel (e.g. 1.4542, 316L) or Ti6Al4V alloy which are predominantly tested in post processed conditions (e.g. machining, heat treatment) in the HCF regime ( $N \leq 10^7$  cycles); the fatigue behavior of as-built specimens has not been investigated intensively. Therefore, valid material values for the fatigue life approach of as-built specimens and SLM parts do not exist. However, for machined specimens fatigue strength is in the range of conventionally manufactured specimens. Standardized fatigue test conditions and

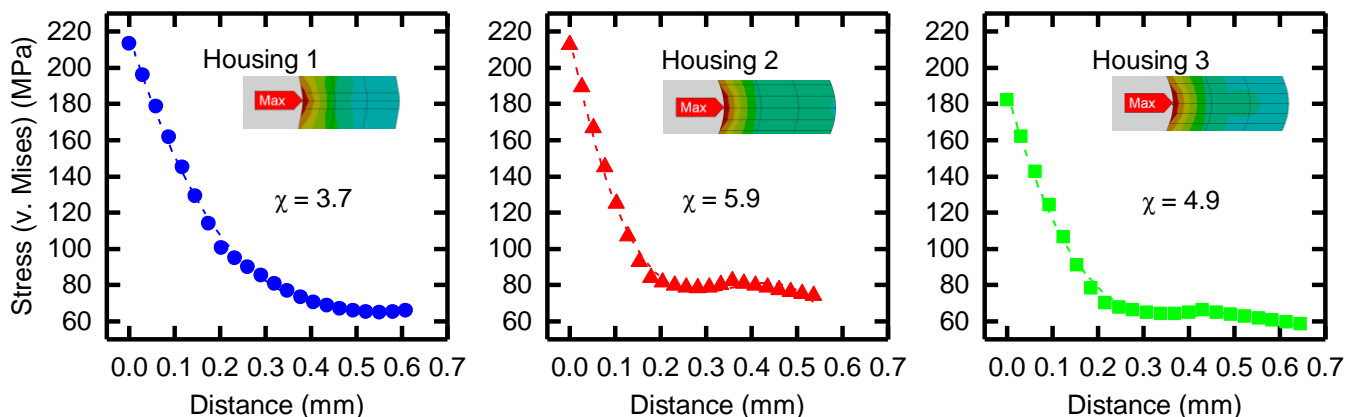


Fig. 7. Stress distribution (v. Mises) of the three different housings under the loads shown in Table 3. Stress distribution is shown in radial direction using FEA. Stress gradient is calculated for notch root ( $x = 0$  mm). Dashed line represents polynomial fit of third order.

documentation (e.g. sample size, test method, statistical analysis, build direction, post processing) for SLM generated specimens might be helpful to ensure comparability between conducted studies.

Experiments on the fatigue behavior of 1.4542 stainless steel as-built and machined specimens as well as of thin-walled as-built actuator housings were performed. A uniaxial test setup with a stress-ratio of  $R = 0$  (pulsating tension) and test runs up to  $N = 10^7$  cycles was selected. From the results the following conclusions can be drawn:

- The fatigue strength at  $N = 10^7$  cycles of as-built specimens ( $\sigma_{max} = 219$  MPa,  $\sigma_a = 110$  MPa) is significantly lower than of machined specimens ( $\sigma_{max} = 492$  MPa,  $\sigma_a = 246$  MPa) due to a high surface roughness. The experimentally determined surface roughness reduction factor  $\gamma$  is 0.44.
- Crack initiation starts for as-built and machined specimens from the surface. Therefore, manufacturing defects in the inside of the SLM generated specimens are not the reason for fatigue failure.
- Machined specimens show a higher sensitivity towards stress in the finite life region compared to as-built specimens. This relation is shown through the slopes of the S-N curves in the relevant cycle regime.
- The endurable peak stress of thin-walled as-built actuator housings at  $10^7$  cycles is significantly above the fatigue strength of as-built specimens (factor 1.57 to 1.94). An explanation can be found in the stress gradient within the thin-walls due to the geometry. Stress gradients  $\chi$  above 3.7 indicate that only a small volume fraction is exposed to high stresses; on average, the stress is significantly below the peak stress. S-N curves support the stress gradient concept that with increasing stress gradient the fatigue strength increases.
- The thin-walled actuator housings demonstrate fatigue strength at  $N = 10^7$  cycles under application relevant loads. In addition, vertical and horizontal scattering of the S-N curves are below the values of the specimens. This allows an approach of fatigue life with a low safety factor.

Future research should be extended to thin-walled housings with other design parameters to prove the stress gradient concept. It is also desired to obtain valid assessment models for fatigue behavior of SLM generated parts without conducting extensive test series.

### Acknowledgments

This work was funded by the LOEWE Research Center AdRIA “Adaptronic Research, Innovation, Application”, grant number III L 4 – 518/14.0004 (2008). The authors would like to thank the Hessen State Ministry of Higher Education, Research and the Arts for the funding.

### References

- Adib-Ramezani, H. and Jeong, J. (2007), “Advanced volumetric method for fatigue life prediction using stress gradient effects at notch roots”, *Computational Materials Science*, Vol. 39 No. 3, pp. 649–663.
- Arola, D. and Williams, C. (2002), “Estimating the fatigue stress concentration factor of machined surfaces”, *International Journal of Fatigue*, Vol. 24 No. 9, pp. 923–930.
- Barbas, A., Bonnet, A.-S., Lipinski, P., Pesci, R. and Dubois, G. (2012), “Development and mechanical characterization of porous titanium bone substitutes”, *Journal of the Mechanical Behavior of Biomedical Materials*, Vol. 9, pp. 34–44.
- Bargel, H.-J. and Schulze, G. (2005), *Werkstoffkunde*, 9., bearb. Aufl, Springer, Berlin [u.a.].
- Bartolo, P., Kruth, J.-P., Silva, J., Levy, G., Malshe, A., Rajurkar, K., Mitsuishi, M., Ciurana, J. and Leu, M. (2012), “Biomedical production of implants by additive electro-chemical and physical processes”, *CIRP Annals - Manufacturing Technology*, Vol. 61 No. 2, pp. 635–655.
- Bathias, C. (1999), “There is no infinite fatigue life in metallic materials”, *Fatigue & Fracture of Engineering Materials and Structures*, Vol. 22 No. 7, pp. 559–565.
- Beretta, S., Clerici, P. and Matteazzi, S. (1995), “The Effect of Sample Size on the Confidence of Endurance Fatigue Tests”, *Fatigue & Fracture of Engineering Materials and Structures*, Vol. 18 No. 1, pp. 129–139.

- Blattmeier, M., Witt, G., Wortberg, J., Eggert, J. and Toepker, J. (2012), "Influence of surface characteristics on fatigue behaviour of laser sintered plastics", *Rapid prototyping journal*, Vol. 18 No. 2, pp. 161–171.
- Brandl, E., Heckenberger, U., Holzinger, V. and Buchbinder, D. (2012), "Additive manufactured AlSi10Mg samples using Selective Laser Melting (SLM): Microstructure, high cycle fatigue, and fracture behavior", *Materials & Design*, Vol. 34, pp. 159–169.
- Buchbinder, D., Schleifenbaum, H., Heidrich, S., Meiners, W. and Bültmann, J. (2011), "High Power Selective Laser Melting (HP SLM) of Aluminum Parts. Lasers in Manufacturing 2011 - Proceedings of the Sixth International WLT Conference on Lasers in Manufacturing", *Physics Procedia*, Vol. 12 No. 0, pp. 271–278.
- Campbell, I., Bourell, D. and Gibson, I. (2012), "Additive manufacturing: rapid prototyping comes of age", *Rapid prototyping journal*, Vol. 18 No. 4, pp. 255–258.
- Chan, K.S., Koike, M., Mason, R.L. and Okabe, T. (2013), "Fatigue Life of Titanium Alloys Fabricated by Additive Layer Manufacturing Techniques for Dental Implants", *Metallurgical and Materials Transactions A*, Vol. 44 No. 2, pp. 1010–1022.
- Chlebus, E., Kuźnicka, B., Kurzynowski, T. and Dybała, B. (2011), "Microstructure and mechanical behaviour of Ti—6Al—7Nb alloy produced by selective laser melting", *Materials Characterization*, Vol. 62 No. 5, pp. 488–495.
- Edwards, P. and Ramulu, M. (2014), "Fatigue Performance Evaluation of Selective Laser Melted Ti-6Al-4V", *Materials Science and Engineering: A*, Vol. 598, pp. 327–337.
- Filippini, M. (2000), "Stress gradient calculations at notches", *International Journal of Fatigue*, Vol. 22 No. 5, pp. 397–409.
- Gibson, I., Rosen, D.W. and Stucker, B. (2010), *Additive manufacturing technologies: Rapid prototyping to direct digital manufacturing*, Springer, New York, NY.
- Gong, H., Rafi, K., Starr, T. and Stucker, B. (2012), "Effect of Defects on Fatigue Tests of As-built Ti-6Al-4V Parts Fabricated by Selective Laser Melting", *Proceedings Solid Freeform Fabrication Symposium 2012, Austin, Texas*, pp. 499–506.
- Grzesiak, A., Becker, R. and Verl, A. (2011), "The Bionic Handling Assistant: a success story of additive manufacturing", *Assembly Automation*, Vol. 31 No. 4, pp. 329–333.
- Gu, D.D., Meiners, W., Wissenbach, K. and Poprawe, R. (2012), "Laser additive manufacturing of metallic components: materials, processes and mechanisms", *International Materials Reviews*, Vol. 57 No. 3, pp. 133–164.
- Huang, S.H., Liu, P., Mokasdar, A. and Hou, L. (2013), "Additive manufacturing and its societal impact: a literature review", *The International Journal of Advanced Manufacturing Technology*, Vol. 67 5-8, pp. 1191–1203.
- Huang, Y. and Leu, M.C. (2014), *Frontiers of Additive Manufacturing Research and Education: An NSF Additive Manufacturing Workshop Report - July 11 and 12, 2013*.
- Hück, M. (1983), "Ein verbessertes Verfahren für die Auswertung von Treppenstufenversuchen", *Materialwissenschaft und Werkstofftechnik*, Vol. 14 No. 12, pp. 406–417.
- Kong, C.-J., Tuck, C.J., Ashcroft, I.A., Wildman, R.D. and Hague, R. (2011), "High Density Ti6Al4V via SLM Processing: Microstructure and Mechanical Properties", *Proceedings Solid Freeform Fabrication Symposium 2011, Austin, Texas*, Vol. 22, pp. 475–483.
- Kruth, J.-P., Badrossamay, M., Yasa, E., Deckers, J., Thijs, L. and van Humbeeck, J. (2010), "Part and material properties in selective laser melting of metals", *Proceedings of the 16th International Symposium on Electromachining*.
- Kuguel, A. (1961), "A relation between theoretical stress concentration factor and fatigue notch factor deduced from the concept of highly stressed volume", *ASTM Proceedings*, Vol. 61, pp. 732–744.
- Lee, J. and Huang, A. (2013), "Fatigue analysis of FDM materials", *Rapid prototyping journal*, Vol. 19 No. 4, pp. 291–299.
- Lee, Y.-L., Pan, J., Hathaway, R.B. and Barkey, M.E. (2005), *Fatigue testing and analysis: Theory and practice*, Elsevier Butterworth-Heinemann, Burlington, Mass.
- Leuders, S., Thöne, M., Riemer, A., Niendorf, T., Tröster, T., Richard, H. and Maier, H. (2013), "On the mechanical behaviour of titanium alloy TiAl6V4 manufactured by selective laser melting: Fatigue resistance and crack growth performance", *International Journal of Fatigue*, Vol. 48, pp. 300–307.

- Lin, S.-K., Lee, Y.-L. and Lu, M.-W. (2001), "Evaluation of the staircase and the accelerated test methods for fatigue limit distributions", *International Journal of Fatigue*, Vol. 23 No. 1, pp. 75–83.
- Lipinski, P., Barbas, A. and Bonnet, A.-S. (2013), "Fatigue behavior of thin-walled grade 2 titanium samples processed by selective laser melting. Application to life prediction of porous titanium implants", *Journal of the Mechanical Behavior of Biomedical Materials*, Vol. 28, pp. 274–290.
- Marines I., Bin, X. and Bathias, C. (2003), "An understanding of very high cycle fatigue of metals", *International Journal of Fatigue*, Vol. 25 9-11, pp. 1101–1107.
- Martin, A., Hinkelmann, K. and Esderts, A. (2011), "Zur Auswertung von Schwingfestigkeitsversuchen im Zeitfestigkeitsbereich. Teil 2: Wie zuverlässig kann die Standardabweichung aus experimentellen Daten geschätzt werden?", *Materials Testing*, Vol. 53 No. 9, pp. 513–521.
- Morrissey, R. and Nicholas, T. (2006), "Staircase testing of a titanium alloy in the gigacycle regime", *International Journal of Fatigue*, Vol. 28 No. 11, pp. 1577–1582.
- Mumtaz, K.A., Erasenthiran, P. and Hopkinson, N. (2008), "High density selective laser melting of Waspaloy®", *Journal of Materials Processing Technology*, Vol. 195 1–3, pp. 77–87.
- Murr, L.E., Quinones, S.A., Gaytan, S.M., Lopez, M.I., Rodela, A., Martinez, E.Y., Hernandez, D.H., Martinez, E., Medina, F. and Wicker, R.B. (2009), "Microstructure and mechanical behavior of Ti–6Al–4V produced by rapid-layer manufacturing, for biomedical applications", *Journal of the Mechanical Behavior of Biomedical Materials*, Vol. 2 No. 1, pp. 20–32.
- Petrovic, V., Vicente Haro Gonzalez, Juan, Jordá Ferrando, O., Delgado Gordillo, J., Ramón Blasco Puchades, Jose and Portolés Griñan, L. (2011), "Additive layered manufacturing: sectors of industrial application shown through case studies", *International Journal of Production Research*, Vol. 49 No. 4, pp. 1061–1079.
- Pyka, G., Kerckhofs, G., Papantoniou, I., Speirs, M., Schrooten, J. and Wevers, M. (2013), "Surface Roughness and Morphology Customization of Additive Manufactured Open Porous Ti6Al4V Structures", *Materials*, Vol. 6 No. 10, pp. 4737–4757.
- Pyttel, B., Schwerdt, D. and Berger, C. (2011), "Very high cycle fatigue – Is there a fatigue limit?", *International Journal of Fatigue*, Vol. 33 No. 1, pp. 49–58.
- Radaj, D. and Vormwald, M. (2007), *Ermüdungsfestigkeit: Grundlagen für Ingenieure*, 3rd ed., Springer, Berlin [u.a.].
- Rafi, H.K., Starr, T.L. and Stucker, B.E. (2013), "A comparison of the tensile, fatigue, and fracture behavior of Ti–6Al–4V and 15-5 PH stainless steel parts made by selective laser melting", *The International Journal of Advanced Manufacturing Technology*, Vol. 69 5-8, pp. 1299–1309.
- Riemer, A., Leuders, S., Thöne, M., Richard, H.A., Tröster, T. and Niendorf, T. (2014), "On the fatigue crack growth behavior in 316L stainless steel manufactured by selective laser melting", *Engineering Fracture Mechanics*, Vol. 120, pp. 15–25.
- Rossow, E. (1964), "Eine einfache Rechenschiebernäherung an die den normal scores entsprechenden Prozentpunkte", *Qualitätskontrolle*, Vol. 9 No. 12, pp. 146–147.
- Schijve, J. (2009), *Fatigue of Structures and Materials*, Springer Netherlands, Dordrecht.
- Sehrt, J.T. and Witt, G. (2010), "Dynamic strength and fracture toughness analysis of beam melted parts", *Proceedings of the 36th International MATADOR Conference*, pp. 385–388.
- Siebel, E. and Stieler, M. (1955), "Ungleichförmige Spannungsverteilung bei schwingender Beanspruchung", *VDI-Z*, Vol. 97 No. 5, pp. 121–126.
- Sonsino, C. (2007), "Course of SN-curves especially in the high-cycle fatigue regime with regard to component design and safety", *International Journal of Fatigue*, Vol. 29 No. 12, pp. 2246–2258.
- Sonsino, C.M. (2008), "Betriebsfestigkeit - Eine Einführung in die Begriffe und ausgewählte Bemessungsgrundlagen", *Materials Testing*, Vol. 50 1-2, pp. 77–90.
- Spickenreuther, M. (2007), "Untersuchungen zur Berechnung der Dauerfestigkeit von randschichtgehärteten Dieseleinspritzdüsen", Dissertation, TU Ilmenau, 2007.
- Spierings, A., Starr, T.L. and Wegener, K. (2013), "Fatigue performance of additive manufactured metallic parts", *Rapid prototyping journal*, Vol. 19 No. 2, pp. 88–94.
- Stanzl-Tschegg, S. (2014), "Very high cycle fatigue measuring techniques", *International Journal of Fatigue*, Vol. 60, pp. 2–17.

- Starr, T., Scherzer, C. and Smith, A. (2011), *Tensile and Fatigue Performance of Laser Sintered Stainless Steels*, SAMPE Direct Part Manufacturing Workshop, Dayton, OH, USA.
- Stoffregen, H.A., Abele, E., Flaschenträger, D. and Melz, T. (2013), “Additive Manufacturing of Reliable Piezoelectric Actuator Modules”, paper presented at 4th Scientific Symposium, CRC/Transregio 39 (PT-PIESA), 26.-27.03.2013, Nürnberg.
- Thijs, L., Montero Sistiaga, Maria Luz, Wauthle, R., Xie, Q., Kruth, J.-P. and van Humbeeck, J. (2013), “Strong morphological and crystallographic texture and resulting yield strength anisotropy in selective laser melted tantalum”, *Acta Materialia*, Vol. 61 No. 12, pp. 4657–4668.
- Thijs, L., Verhaeghe, F., Craeghs, T., van Humbeeck, J. and Kruth, J.-P. (2010), “A study of the microstructural evolution during selective laser melting of Ti–6Al–4V”, *Acta Materialia*, Vol. 58 No. 9, pp. 3303–3312.
- Tolosa, I., Garcíandía, F., Zubiri, F., Zapirain, F. and Esnaola, A. (2010), “Study of mechanical properties of AISI 316 stainless steel processed by “selective laser melting”, following different manufacturing strategies”, *The International Journal of Advanced Manufacturing Technology*, Vol. 51 5-8, pp. 639–647.
- van Hooreweder, B., Coninck, F. de, Moens, D., Boonen, R. and Sas, P. (2010), “Microstructural characterization of SLS-PA12 specimens under dynamic tension/compression excitation”, *Polymer Testing*, Vol. 29 No. 3, pp. 319–326.
- van Hooreweder, B., Moens, D., Boonen, R., Kruth, J.-P. and Sas, P. (2012), “Analysis of Fracture Toughness and Crack Propagation of Ti6Al4V Produced by Selective Laser Melting”, *Advanced Engineering Materials*, Vol. 14 1-2, pp. 92–97.
- van Hooreweder, B., Moens, D., Boonen, R., Kruth, J.-P. and Sas, P. (2013), “On the difference in material structure and fatigue properties of nylon specimens produced by injection molding and selective laser sintering”, *Polymer Testing*, Vol. 32 No. 5, pp. 972–981.
- Wang, F. (2012), “Mechanical property study on rapid additive layer manufacture Hastelloy® X alloy by selective laser melting technology”, *The International Journal of Advanced Manufacturing Technology*, Vol. 58 5-8, pp. 545–551.
- Weibull, W. (1961), *Fatigue testing and analysis of results*, Bergamon Press, Oxford.
- Wu, J.-H. and Lin, C.-K. (2002), “Tensile and fatigue properties of 17-4 PH stainless steel at high temperatures”, *Metallurgical and Materials Transactions A*, Vol. 33 No. 6, pp. 1715–1724.
- Wycisk, E., Emmelmann, C., Siddique, S. and Walther, F. (2013), “High Cycle Fatigue (HCF) Performance of Ti-6Al-4V Alloy Processed by Selective Laser Melting”, *Advanced Materials Research*, 816-817, pp. 134–139.
- Zhai, Y., Lados, D.A. and LaGoy, J.L. (2014), “Additive Manufacturing: Making Imagination the Major Limitation”, *JOM*, Vol. 66 No. 5, pp. 808–816.